Inorganic Chemistry

Article

Cite This: Inorg. Chem. 2017, 56, 13822-13828

pubs.acs.org/IC

Organoarsonate Functionalization of Heteropolyoxotungstates

Xiaofeng Yi,[†,‡] Natalya V. Izarova,[†] and Paul Kögerler*[,†,‡]

[†]Jülich-Aachen Research Alliance (JARA-FIT) and Peter Grünberg Institute, PGI 6, Forschungszentrum Jülich, D-52425 Jülich, Germany

[‡]Institute of Inorganic Chemistry, RWTH Aachen University, D-52074 Aachen, Germany

Supporting Information

ABSTRACT: Functionalization of the $\{P_8W_{48}\}$ polyoxotungstate (POT) archetype with aromatic organoarsonates results in the first homometallic $\{P_8W_{48}\}$ derivatives, with the general formula $[(RAs^{V}O)_4P^{V}{}_8W^{VI}{}_{48}O_{184}]^{32-}$ [R = C_6H_5 (**1**) or *p*-$(H_2N)C_6H_4$ (**2**)]. Short As−O bonds here induce unusual bending of the otherwise rigid $\{P_8W_{48}\}$ macrocycle, breaking its D_{4h} symmetry. The obtained species also represent the first lacunary POTs functionalized with organoarsonates and can potentially act as polyoxometalate precursors themselves. We elaborate solution stability in different aqueous media using ^{1}H and ^{31}P NMR spectroscopy and possible pathways for subsequent transformations in aqueous solutions of the functionalized polyanions. Recrystallization of the K^+/Li^+/dimethylammonium salt of **2** from 4 M LiCl solution yielded a further functionalized POT, $[(H_3NC_6H_4AsO)_3P_8W_{48}O_{184}H_x\{WO_2(H_2O)_2\}_{0.4}]^{(30.2-x)-}$ (**3**), revealing dissociation of the organoarsonate fragments in slightly acidic aqueous solutions followed by their rearrangement within the inner POT cavity.

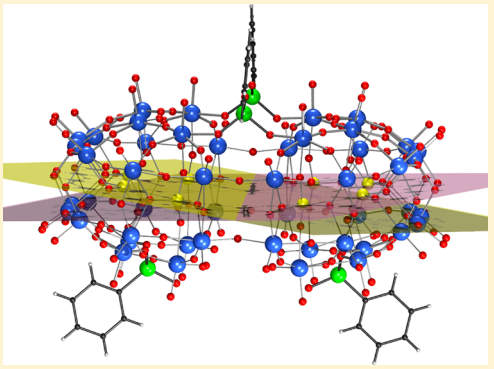

1. INTRODUCTION

The combination of structural versatility, redox robustness, and the ability to act as multidentate ligands toward oxophilic heterometals renders polyoxotungstates (POTs), a large family of discrete polynuclear oxo complexes of W^{VI} and W^{V} ions, highly attractive for application in many areas ranging from catalysis, electrochemistry, photochromism, and magnetism to medicine.[1] Further expansion of these clusters' structural diversity can be achieved by their functionalization with organic moieties, e.g., organosilyl, organophosphonate and -phosphoryl, organotin, and other groups.[2]

Until now, the reactivity of organoarsenic-based reagents toward POTs has received relatively little attention. While a series of organoarsinates $[R_2As^{V}Mo^{VI}{}_4O_{15}H]^{2-}$ (R = CH_3, C_2H_5, C_6H_5)[3] and organoarsonate-functionalized polyoxomolybdates with formulas $[(RAs^{V}O_3)_4Mo^{VI}{}_4O_{10}]^{4-}$,[4h,q] $[(RAs^{V}O_3)_2Mo^{VI}{}_5O_{15}]^{4-}$,[4e] $[(MeAs^{V}O_3)Mo^{VI}{}_6O_{18}(H_2O)_6]^{2-}$,[3b] $[(RAs^{V}O_3)_2Mo^{VI}{}_6O_{18}]^{4-}$,[4a,d,e,h,l] $[(RAs^{V}O_3)_2Mo^{VI}{}_6O_{19}H_x]^{(6-x)-}$,[4b,f,g] $[(PhAs^{V}O_3)Mo^{VI}{}_7O_{22}]^{4-}$,[4d] and $[(RAs^{V}O_3)_4Mo^{VI}{}_{12}O_{34}]^{4-}$,[4c,i−m,o] and several Mo^{V}-based and mixed-valent $Mo^{V/VI}$ species[4n,p,q] [R = CH_3, *n*-C_3H_7, C_6H_5, $C_6H_4(CH_3)$, *p*-$C_6H_4(NH_2)$, *p*-$C_6H_4(OH)$, *p*-$C_6H_4(COOH)$, *p*-$C_6H_4(CN)$, *o*-$C_6H_4(NO_2)$, C_6H_3-4-OH-3-NO_2, C_6H_3-4-OH-3-$N(H)C(O)CH_3$, etc.] are known, organoarsonate-containing POTs are restricted to the isopolyoxotungstate derivatives $[(RAs^{V}O_3)_2W_6O_{18}]^{6-}$ and $[(RAs^{V}O_3)W_7O_{24}H]^{7-}$.[4k,5] These species were obtained by the direct condensation of tungstate ions with organoarsonates in aqueous media (pH 5−8).

In order to prepare novel hybrid polyanions offering the potential for subsequent integration of magnetic metal ions, we explored the reactivity of organoarsonates with multilacunary POTs. The seminal, highly stable macrocyclic POT $[H_7P_8W_{48}O_{184}]^{33-}$ ($\{P_8W_{48}\}$)[6] was chosen for these experiments because it is regarded as highly stable and comparably inert toward substitution of its phosphate heterogroups and provides adequate coordination sites between its four $\{P_2W_{12}O_{48}\}$ building blocks. In $\{P_8W_{48}\}$, the latter are linked by oxo bridges into a wheel-shaped structure with a large inner cavity (approximately 1 nm in diameter), able to accommodate various transition and rare-earth metals as well as their oxo/hydroxo clusters, e.g., in $[Cu_{20}X(OH)_{24}(H_2O)_{12}P_8W_{48}O_{184}]^{25-}$ (X = Cl, Br, I), $[Cu_{20}(N_3)_6(OH)_{18}P_8W_{48}O_{184}]^{24-}$, and $[K_8\subset\{P_8W_{48}O_{184}\}\{Mo^{VI}O_2\}_4\{Mo^{V}{}_4O_{10}(H_2O)_3\}_2]^{24-}$.[7] Moreover, it can act as a secondary building block in numerous fully inorganic coordination polymers, as exemplified by the 3D framework compounds $K_{18}Li_6[Mn_8(H_2O)_{48}P_8W_{48}O_{184}]\cdot 108H_2O$ with huge rigid voids[8] or the recently reported $Li_9K_7W_1Co_{10}[H_2P_8W_{48}O_{186}]\cdot nH_2O$, which can undergo several crystal-to-crystal transformations, resulting in structures of different connectivities (from 0D up to 3D).[9] An additional advantage of $\{P_8W_{48}\}$ as the precursor for further functionalization is its solubility and stability in aqueous solutions in the unusually broad pH range from 1 to 8.[6]

Very recently, we have reported the first examples of $\{P_8W_{48}\}$ complexes with the main-group metals $[K_{4.5}\subset(ClSn^{II})_8P_8W_{48}O_{184}]^{17.5-}$ and $[(HOSn^{II})_6P_8W_{48}O_{184}]^{34-}$.[10] At the same time, to our knowledge, no $\{P_8W_{48}\}$

Received: July 28, 2017
Published: November 9, 2017

DOI: 10.1021/acs.inorgchem.7b01928
Inorg. Chem. 2017, 56, 13822−13828

derivatives with nonmetal elements are known. We here report two $[(RAs^{V}O)_4P^{V}{}_8W^{VI}{}_{48}O_{184}]^{32-}$ polyanions with R = C_6H_5 (**1**) and *p*-$(H_2N)C_6H_4$ (**2**) that represent not only the first homometallic $\{P_8W_{48}\}$ derivatives but also the first lacunary POTs functionalized with organoarsonates possessing the potential to act as precursors for organoarsonate-functionalized heterometal polyoxometalate (POM) complexes.

2. EXPERIMENTAL SECTION

2.1. General Methods and Materials. The starting reagents were used as purchased without further purification. $K_{28}Li_5[H_7P_8W_{48}O_{184}]\cdot 92H_2O$ (**KL-**$\{\mathbf{P_8W_{48}}\}$) was synthesized according to the published procedure,[6] and its identity and purity were confirmed by IR and ^{31}P NMR spectroscopy. Elemental analysis results [inductively coupled plasma atomic emission spectroscopy (ICP-OES) and C, H, and N] were obtained from the Central Institute for Engineering, Electronics and Analytics (ZEA-3), Forschungszentrum Jülich GmbH (Jülich, Germany). Thermogravimetric/differential thermal (TGA/DTA) analysis measurements were carried out with a Mettler Toledo TGA/SDTA 851 in dry N_2 (60 mL min^{-1}) at a heating rate of 5 K min^{-1}. Vibrational spectra were recorded on a Bruker Vertex 70 Fourier transform infrared (FT-IR) spectrometer coupled with a RAM II FT-Raman module (1064 nm Nd:YAG laser) on KBr disks for the FT-IR measurements and a solid material for the Diamond ATR FT-IR and Raman measurements. ^1H and ^{31}P NMR spectra were recorded at room temperature in 5 mm tubes using a Bruker Avance 600 MHz spectrometer equipped with a prodigy probe, operating at 600.15 MHz for ^1H and 242.95 MHz for ^{31}P, and with a Varian Inova 400 MHz spectrometer equipped with an Auto-X-PFG probe, using a resonance frequency of 161.834 MHz for ^{31}P. Chemical shifts are reported with respect to $Si(CH_3)_4$ (^1H) and 85% H_3PO_4 (^{31}P); all chemical shifts downfield of the reference are reported as positive values. The solid-state ^{31}P magic-angle-spinning (MAS) NMR measurements were performed at ambient temperature using a Bruker AVANCE III spectrometer with a 9.4 T magnetic field. The spectrometer was equipped with a Bruker triple resonance probe for rotors of 2.5 mm diameter. The ground sample powder was filled into a ZrO_2 rotor for experiments with and without sample spinning. Rotation frequencies of 35 and 15 kHz were applied during MAS. Eight-fold cyclization of the pulse sequences with a cycle delay of 120 s was used. The signal shift is referred to H_3PO_4.

2.2. Synthetic Procedures. *Synthesis of* $K_8Li_{17}[(CH_3)_2NH_2]_7[(C_6H_5AsO)_4P_8W_{48}O_{184}]\cdot 130H_2O$ *(**KLD-1**).* A solution of $C_6H_5AsO_3H_2$ (0.0505 g, 0.25 mmol) in 5 mL of 1 M LiCl with pH 2.2 adjusted by glacial acetic acid was added dropwise to a solution of **KL-**$\{\mathbf{P_8W_{48}}\}$ (0.37 g, 0.025 mmol) in 15 mL of 1 M LiCl under vigorous stirring. The obtained reaction mixture with pH 3.0 was then placed in an oven and heated at 60 °C for 4 days. After cooling to room temperature, aqueous 1 M $[(CH_3)_2NH_2]Cl$ (20 drops) was added to the resulting solution and left for evaporation (pH 2.97). Transparent colorless blocklike crystals of **KLD-1** formed in 2 weeks. The pH of the solution after crystallization remained unchanged at 2.96. The crystals were collected by filtration and dried in air. Yield: 0.134 g (34 % based on $\{P_8W_{48}\}$). Elem anal. Calcd for $C_{38}H_{336}As_4K_8Li_{17}N_7O_{318}P_8W_{48}$ (found), mass %: C, 2.89 (2.90); H, 2.15 (2.25); As, 1.90 (1.94); K, 1.98 (1.87); Li, 0.75 (0.78); N, 0.62 (0.66); P, 1.57 (1.55); W, 55.91 (53.9). IR (KBr pellets, cm^{-1}): 3438 (s, br), 1633 (s), 1461 (w), 1438 (w), 1135 (m), 1083 (m), 1022 (m), 939 (s), 820 (s), 727 (s), 667 (s), 466 (s). Raman (solid sample, λ_e = 1064 nm, cm^{-1}): 1003 (w), 969 (s), 886 (m), 637 (m), 388 (w), 214 (m). ^1H NMR (D_2O): 7.72 (d, 2H), 7.61 (m, 1H), 7.54 (m, 2H).

Synthesis of $K_{10.5}Li_{14}[(CH_3)_2NH_2]_{3.5}[(H_3NC_6H_4AsO)_4P_8W_{48}O_{184}]\cdot 92H_2O$ *(**KLD-2**).* A solution of *p*-$(H_2N)C_6H_4AsO_3H_2$ (0.0542 g, 0.25 mmol) in 5 mL of 1 M LiCl with pH 2.2 adjusted by glacial acetic acid was added dropwise to a solution of **KL-**$\{\mathbf{P_8W_{48}}\}$ (0.37 g, 0.025 mmol) in 15 mL of 1 M LiCl with vigorous stirring. The obtained reaction mixture with pH 3.0 was then placed in an oven and heated at 60 °C for 4 days. After cooling to room temperature, 8 drops of aqueous 1 M $[(CH_3)_2NH_2]Cl$ was added to the yellowish reaction mixture, and the resulting solution was left for evaporation (pH 3.03). Light-yellow crystals of **KLD-2** formed after 1 week. The pH of the solution after crystallization remained virtually unchanged at 2.98. The product was collected by filtration and dried in air. Yield: 0.154 g (41 % based on $\{P_8W_{48}\}$). Elem anal. Calcd for $C_{31}H_{240}As_4K_{10.5}Li_{14}N_{7.5}O_{280}P_8W_{48}$ (found), mass %: C, 2.47 (2.46); H, 1.60 (1.59); As, 1.99 (1.95); K, 2.72 (2.68); Li, 0.64 (0.62); N, 0.70 (0.77); P, 1.64 (1.62); W, 58.52 (58.02). IR (KBr pellets, cm^{-1}): 3422 (s, br), 1629 (s), 1496 (w), 1465 (w), 1413 (w), 1324 (w), 1135 (m), 1085 (m), 1023 (m), 935 (s), 833 (s), 728 (s), 671 (s), 464 (s). Raman (solid sample, λ_e = 1064 nm, cm^{-1}): 966 (s), 877 (m), 802 (w), 708 (m), 633 (m), 382 (w), 313 (w), 204 (m). ^1H NMR (D_2O): 7.50 (d, 2H), 6.88 (d, 2H).

Synthesis of $K_{7.2}Li_{23-x}[(H_3NC_6H_4AsO)_3P_8W_{48}O_{184}H_x\{WO_2(H_2O)_2\}_{0.4}]\cdot nH_2O$ *(**KL-3**).* A sample of **KLD-2** (0.040 g, 0.003 mmol) was dissolved in aqueous 4 M LiCl (22 mL) with heating at 70 °C for 40 min. After that, the solution (pH 2.7) was divided into four vials and left for evaporation at room temperature. Needlelike crystals of **KL-3** started to form after 1 week. The crystals were collected by filtration and dried in air. Yield: 0.021 g. IR (KBr pellets, cm^{-1}): 3440 (s, br), 1629 (s), 1497 (w), 1416 (w), 1326 (w), 1294 (w), 1135 (m), 1083 (m), 1022 (m), 937 (s), 816 (s), 677 (s), 464 (s). Raman (solid sample, λ_e = 1064 nm, cm^{-1}): 969 (s), 890 (m), 801 (w), 695 (m), 633 (m), 370 (w), 320 (w), 207 (m).

*2.2.4. Synthesis of **KL-4**.* A sample of **KLD-2** (0.040 g, 0.003 mmol) was dissolved in aqueous 4 M LiCl (20 mL), followed by the addition of $FeCl_3\cdot 6H_2O$ (0.006 g, 0.021 mmol), while the reaction mixture was stirred at 70−100 °C for 1 h. The resulting solution with pH 2.2 was filtered while hot to remove a small amount of fine precipitate. The filtrate produced a yellow precipitate after cooling, which was collected the next day. Elem anal. (ICP-OES): Fe:As:P:W = 7.7:4:8:48. IR (KBr pellets, cm^{-1}): 3434 (s, br), 1635 (s), 1496 (w), 1417 (w), 1322 (w), 1144 (m),1084 (m), 1020 (m), 935 (s), 916 (s), 796 (s), 723 (s), 470 (s).

Single-crystal diffraction data for **KLD-1**, **KLD-2**, and **KL-3** were collected on a SuperNova (Agilent Technologies) diffractometer at 120 K with Mo Kα radiation (λ = 0.71073 Å) for **KLD-1** and Cu Kα radiation (λ = 1.54184 Å) for **KLD-2** and **KL-3**. The crystals were mounted in a Hampton cryoloop with Paratone-N oil to prevent water loss. Absorption corrections was applied numerically based on Gaussian integration over a multifaceted crystal model.[2] The *SHELXTL* software package[3] was used to solve and refine the structures. The structures were solved by direct methods and refined by a full-matrix least-squares method against $|F|^2$ with anisotropic thermal parameters for all heavy atoms (As, K, P, and W) with application of ISOR instructions for the refinement of some heavily disordered K cations. The K^+ counterions in the structure of **KL-3** with the site occupancy factor less than 0.25 were refined in isotropic approximation. The relative site occupancy factors for the disordered positions of the K cations as well as O atoms of the crystal water molecules were first refined in an isotropic approximation with U_{iso} = 0.05, then fixed at the obtained values, and refined without thermal parameter restrictions. No Li^+ positions and H atoms of the crystal water molecules have been located. H atoms of the phenyl rings of the $PhAsO_3^{2-}$ and *p*-arsanilate ligands and the amino and methyl groups of *p*-arsanilates and the located dimethylammonium cations, respectively, were placed in geometrically calculated positions. Because of severe disorder, only 4 DMA^+ cations could be located in the structure of **KLD-1** and no DMA^+ cations in the structure of **KLD-2**, while 7 and 3.5 DMA^+ counterions are present in these structures, respectively, based on elemental analysis. Because of this disorder, there are only 15 highly disordered water molecules in **KLD-1** (with O site occupancy from 0.0625 to 0.5) out of 130, the number determined from elemental analysis and TGA for this compound. Similarly, the O positions for only 18.5 out of 92 water molecules were located in the structure of **KLD-2**. This is consistent with the large solvent-accessible volume remaining in the structures. For the overall consistency, the final formulas in the crystallographic data correspond to the compositions of the bulk materials determined by elemental analysis and TGA. The rather high values of R_{int} for **KLD-1**, **KLD-2**, and **KL-3**

DOI: 10.1021/acs.inorgchem.7b01928
Inorg. Chem. 2017, 56, 13822−13828

Table 1. Crystallographic Data and Structure Refinement Details for KLD-1, KLD-2, and KL-3

sample	KLD-1	KLD-2	KL-3
radiation source	Mo Kα	Cu Kα	Cu Kα
empirical formula	$C_{38}H_{336}As_4K_8Li_{17}N_7O_{318}P_8W_{48}$	$C_{31}H_{240}As_4K_{10.5}Li_{14}N_{7.5}O_{280}P_8W_{48}$	$C_{18}H_{215.6}As_3K_{7.2}Li_{17}N_3O_{283.6}P_8W_{48.4}$
fw, g mol^{-1}	15784.16	15079.26	14783.50
cryst syst	tetragonal	triclinic	triclinic
space group	$I\bar{4}$	$P\bar{1}$	$P\bar{1}$
a, Å	25.1943(1)	23.0426(7)	14.4150(6)
b, Å	25.1943(1)	24.3124(7)	21.7712(7)
c, Å	25.6924(3)	29.9784(8)	24.5919(6)
α, deg	90	80.834(2)	69.384(3)
β, deg	90	82.616(2)	78.910(3)
γ, deg	90	14949.4(7)	82.697(3)
volume, Å^3	16308.3(2)	14949.4(7)	7073.8(4)
Z	2	2	1
D_{calcd}, g cm^{-3}	3.214	3.350	3.470
abs coeff, mm^{-1}	17.519	36.373	38.142
$F(000)$	14328	13528	6602
cryst size, mm^3	0.28 × 0.29 × 0.32	0.06 × 0.08 × 0.24	0.06 × 0.09 × 0.33
θ range for data collection	4.10−25.67	8.88−66.59	8.95−65.09
completeness to θ_{max}, %	99.5	99.5	99.3
index ranges	$-30 < h < +30$, $-30 < k < +30$, $-31 < l < +31$	$-27 < h < +27$, $-28 < k < +28$, $-35 < l < +35$	$-16 < h < +16$, $-24 < k < +25$, $-28 < l < +28$
reflns collected	153179	262401	94589
indep reflns	15399	52558	23947
R_{int}	0.1239	0.1341	0.1351
obsd [$I > 2\sigma(I)$]	13962	32564	15078
abs corrn	numerical based on Gaussian integration over a multifaceted crystal model		
T_{min}/T_{max}	0.0118/0.0844	0.0130/0.2352	0.0120/0.2044
no. of data/restraints/param	15399/32/469	52558/48/1716	23947/0/869
GOF on F^2	1.042	1.035	1.031
R_1, wR_2 [$I > 2\sigma(I)$]	0.0487, 0.1280	0.0921, 0.2304	0.0842, 0.2142
R_1, wR_2 (all data)	0.0562, 0.1360	0.1457, 0.2771	0.1339, 0.2628
largest diff peak/hole, e Å^{-3}	2.486/−1.409	4.387/−2.824	3.308/−2.972

(0.124, 0.134, and 0.135, respectively), combined with several violations of systematic absences, are consistent with the twinning issue (especially considering the needlelike shape of the crystals). Because we were unable to discern any pattern in the list of reflections for which $F(obs) \gg F(calc)$, we were not able to systematically remove composite reflections. Additional crystallographic data are summarized in Table 1.

3. RESULTS AND DISCUSSION

3.1. Syntheses and Crystal Structures. Polyanions **1** and **2** have been prepared by heating of **KL-{P_8W_{48}}** with phenylarsonic (**1**) or *p*-arsanilic (**2**) acid in a 1 M LiCl solution (pH 3.0) at 60 °C. The pH of the reaction mixture was adjusted by the addition of glacial acetic acid to the initial organoarsonate solution. On the one hand, this slightly improves the solubility of the organoarsonic acids in a 1 M LiCl medium. On the other hand, it reduces pH fluctuations while mixing the $[P_8W_{48}O_{184}]^{40-}$ and organoarsonate ligand solutions compared to directly mixing the reagents in 1 M aqueous LiCl followed by the addition of acetic acid to the final mixture. **1** and **2** crystallize as the hydrated mixed potassium/lithium/dimethylammonium (DMA^+) salts $K_8Li_{17}[(CH_3)_2NH_2]_7[(C_6H_5AsO)_4P_8W_{48}O_{184}]\cdot 130H_2O$ (**KLD-1**) and $K_{10.5}Li_{14}[(CH_3)_2NH_2]_{3.5}[(H_3NC_6H_4AsO)_4P_8W_{48}O_{184}]\cdot 92H_2O$ (**KLD-2**) in the tetragonal $I\bar{4}$ and triclinic $P\bar{1}$ space groups, respectively. The precise numbers of K^+, Li^+, and DMA^+ countercations as well as crystal water molecules in **KLD-1** and **KLD-2** were established from elemental and thermogravimetric analyses. **1** and **2** can also be crystallized with Rb^+ and Cs^+ countercations instead of DMA^+; however, **1** and **2** cannot be isolated directly from the reaction mixture without additional counterions.

Single-crystal X-ray diffraction reveals that the structures of **1** and **2** comprise four {RAs^VO} units [R = C_6H_5 (**1**) and *p*-$(H_2N)C_6H_4$ (**2**)] that are covalently bound to the two inner rims of the {P_8W_{48}} wheel through As−O−W bonds (Figures 1 and S1). The As^V ions of the {RAs^VO} groups in **1** and **2** occupy four of the eight available vacant sites of {P_8W_{48}}, and each coordinates to two O atoms belonging to two adjacent {P_2W_{12}} units [As−O = 1.683(12)−1.718(12) Å in **1** and 1.671(19)−1.73(2) Å in **2**]. The tetragonal As^V coordination sphere is completed by a terminal oxo ligand [As−O = 1.661(15) Å in **1** and 1.63(2)−1.68(3) Å in **2**] and a C atom of the phenyl (**1**) or *p*-aminophenyl (**2**) group [As−C = 1.891(9) Å in **1** and 1.883(16)−1.930(17) Å in **2**]. The aromatic rings are directed outward from the inner cavity of the polyanion, minimizing potential steric hindrances (Figures 1 and S1). The bond lengths and angles within the {P_8W_{48}} framework and organic moieties are in the usual ranges (see Table S2). Two As^V ions occupy opposite (alternating) coordination sites on one rim of the POT wheel, while the other two are located on the other rim, binding to opposite vacant sites, which are in orthogonal positions to the first two (Figure 1b, right),

DOI: 10.1021/acs.inorgchem.7b01928
Inorg. Chem. 2017, 56, 13822−13828

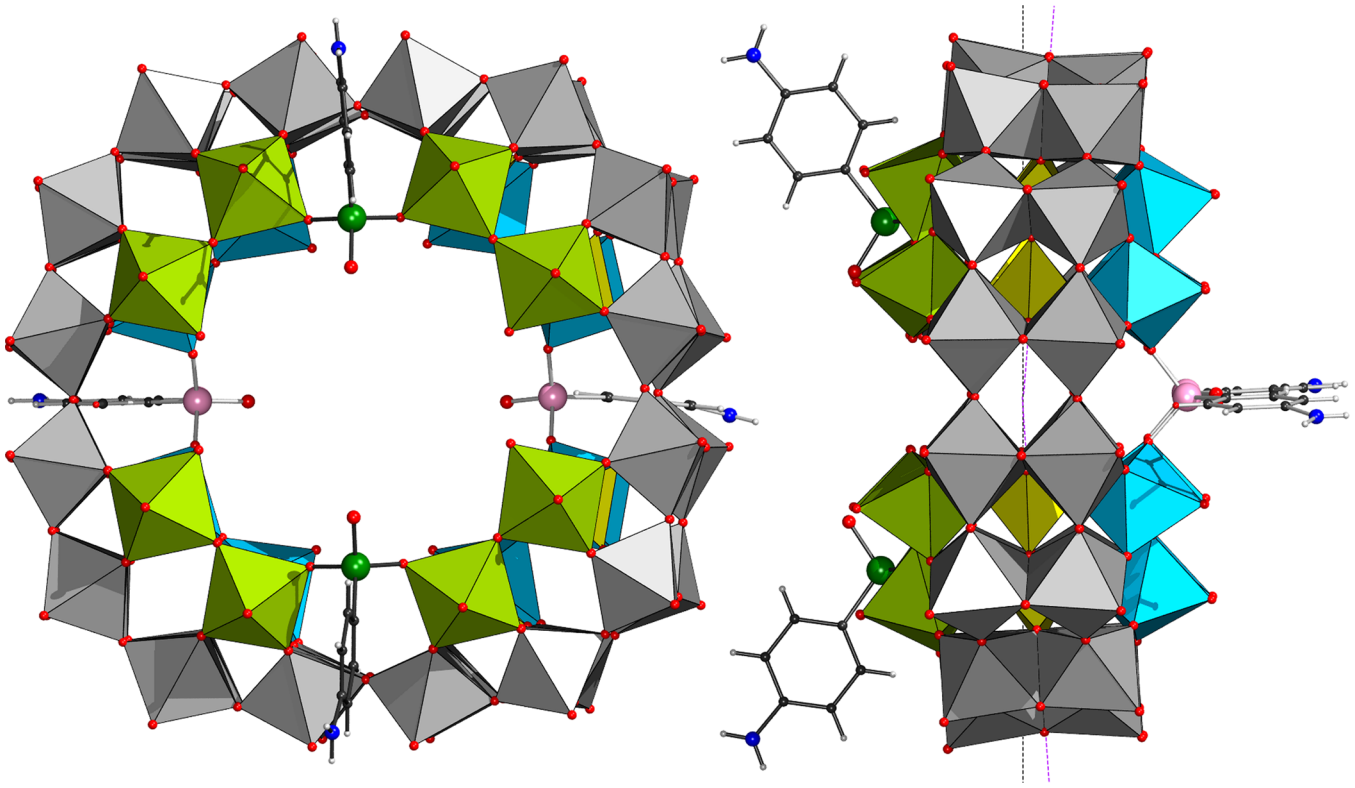

Figure 1. Structures of polyanion **2** in perpendicular views. WO_6 octahedra of the front (lime green) and rear (light blue) inner rims of the $\{P_8W_{48}\}$ wheel defining the coordination sites for the *p*-arsanilate groups (in a ball-and-stick representation; front-facing $H_2NPhAsO$ groups, dark-gray bonds; As, dark green; rear-facing groups, light-gray bonds; As, rose). Dashed lines indicate deviation from the planar regular structure of $\{P_8W_{48}\}$. Color code: WO_6, gray; PO_4, yellow polyhedra; C, black; N, blue; O, red spheres. Some H atoms are omitted for clarity. See Figure S1 for the structure of **1**.

resulting in approximately C_{2v} symmetry (if slight rotations of the phenyl and *p*-aminophenyl groups are not considered).

Relatively short As−O bonds compared to the M−O bonds in the complexes of $\{P_8W_{48}\}$ with heterometals (1.9−2.3 Å) cause slight distortions within the $\{P_8W_{48}\}$ skeleton. Thus, the macrocyclic wheel is somewhat tilted toward two $\{RAs^VO\}$ units (Figure 1b, right): the O···O distance between the two O ions coordinated to one As^V constitutes 2.65 Å for **1** and is in the range from 2.63 to 2.68 Å for **2**, while the O···O distance between the corresponding O centers of the noncoordinated vacant sites is 3.39 Å for **1** and 3.21−3.36 Å for **2**. This distortion probably limits the number of incorporated $\{RAs^VO\}$ groups to four (vs eight), even if larger L/POT ratios are used in the reaction mixture (e.g., 20:1 instead of 10:1), and is responsible for the geometry of the complexes because coordination of the $\{RAs^VO\}$ groups at the four specific positions allows minimization of the strain within the POT skeleton. Charge neutrality for **KLD-2** requires the presence of four protons. The bond-valence-sum calculations[11] indicate that these protons are not likely associated with any of the O atoms of the polyanion (see Table S3 for details). At the same time, the relatively low pH used in the synthesis of **2** suggests protonation of the amino groups of the *p*-arsanilate ligands, similar to the situation observed for the *p*-arsanilate-functionalized polyoxomolybdates.[4k]

3.2. Solution Studies. The solution behaviors of **1** and **2** in aqueous media have been examined by ^1H and ^{31}P NMR spectroscopy. The ^1H NMR spectrum of a **KLD-1** solution in D_2O (Figure S7) exhibits that expected for the phenyl ring combination of a doublet (7.72 ppm) and two triplets (7.61 and 7.54 ppm) in an approximate 2:1:2 integral ratio. The ^1H NMR spectrum of a D_2O solution of **KLD-2** (Figure S8) shows two doublets (7.565 and 6.97 ppm) corresponding to the two pairs of symmetrically equivalent protons of the phenyl rings of the *p*-arsanilate ligands, while the signal of the NH_2 group protons overlaps with the strong H_2O signal. The signals in the spectra of **1** and **2** are significantly shifted compared to those of noncoordinated phenylarsonate [7.765 (d), 7.70 (t), and 7.60 (t) ppm] and *p*-arsanilate [7.565 (d) and 6.97 (d) ppm] anions (Figures S7 and S8), indicating the stability of **1** and **2** in an aqueous medium over the short time period of the ^1H NMR measurement.

The solution stability over longer time periods (1 h to 1 day) has been studied using ^{31}P NMR spectroscopy. On the basis of the crystal structures of **KLD-1** and **KLD-2**, we expect only a singlet for both polyanions in case they are intact in solution. In addition, two overlapping signals at −6.9 and −7.1 ppm as well as a wider signal contribution downfield to these signals were observed in the solid-state ^{31}P MAS NMR spectrum for **KLD-1** (at a rotation frequency of 15 kHz; Figure S9). The appearance of several signals is most likely due to disorder of K^+ cations bound in the inner cavity of the polyanion to phosphate O atoms that in the crystal lattice renders phosphates bound and not bound to K^+ nonequivalent. Solution ^{31}P NMR spectra were measured at room temperature in several media of various basicity and ionic strength, such as H_2O (Figures S10 and S11), 1 M $LiCl_{aq}$ (Figures S12 and S13), 4 M $LiCl_{aq}$ (Figures S14 and S15), 2 M Li_2SO_4/H_2SO_4 buffer (pH 3.0; Figures S16 and S17), 0.5 M LiOAc (pH 6.76, Figures S18 and S19), and 2 M LiOAc (pH 7.6; Figures S20 and S21) solutions as well as 0.5

DOI: 10.1021/acs.inorgchem.7b01928
Inorg. Chem. 2017, 56, 13822−13828

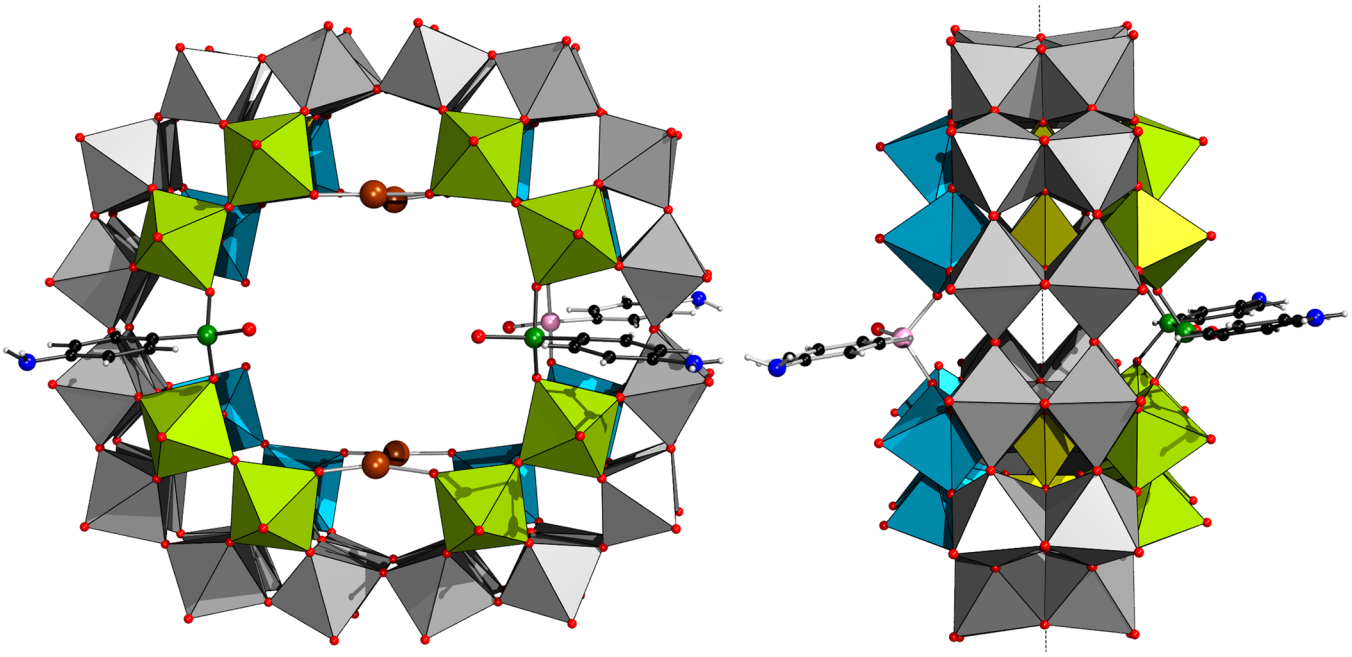

Figure 2. Structures of polyanion **3** in perpendicular views. The color code is as in Figure 1. The four additional underoccupied W^{VI} centers (sof 0.1) are shown as brown spheres, and their terminal O and H_2O groups could not be located due to low occupancy.

M Tris buffer with pH 7.6 (Figures S22 and S23). While the compounds were well-soluble in water, heating has to be applied to dissolve **KLD-1** and **KLD-2** in Li-based media and in Tris buffer. Already 1 h after redissolution, the spectra of **1** and **2** in H_2O and all Li-based media exhibit two sets of closely spaced signals: one at around −6.5/−7 ppm, and the other one slightly shifted upfield, while the exact positions, number, and relative intensities of these signals are changed after 1 day. These results are evident of at least partial decomposition of the polyanions, which most likely occurs by dissociation of the organoarsonate ligands. The cleanest spectra in these media and, in turn, best stability against hydrolysis were observed in 4 M LiCl solutions after 1 h, which exhibit main signals at −7.1 ppm (for **1**) and −6.7 ppm (for **2**), along with small upfield peaks at −7.6 ppm (**1**) and −7.3 ppm (**2**) (Figures S14 and S15), which compare well with the chemical shifts in the solid state and differ from the chemical shift for the P atoms of the noncoordinated $\{P_8W_{48}\}$ wheels in this medium (−6.9 ppm). However, after 1 day, the spectrum of the same solution shows several overlapping signals, similar to the results obtained in the other tested media.

At the same time, the spectra of **KLD-1** and **KLD-2** solutions in 0.5 M Tris buffer (pH 7.6) exhibit a singlet at −8.3 and −8.4 ppm, respectively, after 1 h, 4 h, and 1 day. The chemical shifts unambiguously differ from the signal at −8.0 ppm observed for non-functionalized $\{P_8W_{48}\}$ in the same medium appearing along with additional small peaks, which strongly supports at least one-day stability of the organoarsonate $\{P_8W_{48}\}$ derivatives **1** and **2** in this medium. Thus, the above results point to a significant potential of **1** and **2** to act as novel organically functionalized POM precursors in Tris aqueous solutions at pH 7−8.

3.3. Recrystallization and Complexation with Heterometal Experiments. For further insight into the hydrolysis processes in the LiCl media, we analyzed crystals isolated from the solution of **KLD-2** in 4 M LiCl. Structural analysis revealed the composition $K_{7.2}Li_{23-x}[(H_3NC_6H_4AsO)_3P_8W_{48}O_{184}H_x\{WO_2(H_2O)_2\}_{0.4}]\cdot nH_2O$ (**KL-3**). The three As^V centers in the polyanion **3** bind to O atoms of the vacant sites situated on opposite rims of the $\{P_8W_{48}\}$ wheel (Figure 2). The two inversion-symmetric As^V positions are fully occupied, while the remaining As^V ion (along with its *p*-aminophenyl and terminal oxo ligands) is disordered over the two remaining positions with equal occupancy. This means that either (a) only a single $[(H_3NC_6H_4AsO)_3P_8W_{48}O_{184}H_x\{WO_2(H_2O)_2\}_{0.4}]^{(30.2-x)-}$ polyanion type makes up the crystals of **KL-3** (with three monoprotonated *p*-arsanilate ligands bound to the $\{P_8W_{48}\}$ macrocycle) or (b) there is an equimolar mixture of species with two and four organoarsonates, $[(H_3NC_6H_4AsO)_2P_8W_{48}O_{184}H_x\{WO_2(H_2O)_2\}_{0.4}]^{(33.2-x)-}$ and $[(H_3NC_6H_4AsO)_4P_8W_{48}O_{184}H_x\{WO_2(H_2O)_2\}_{0.4}]^{(27.2-x)-}$, respectively. The additional four vacant sites of $\{P_8W_{48}\}$ in **3** are surprisingly occupied by W^{VI} centers (with a relative site occupancy factor of 0.1), which is related to minor $\{P_8W_{48}\}$ decomposition during heating. This result shows that the $\{RAs^VO\}$ groups in **1** and **2** readily dissociate in slightly acidic aqueous solutions, followed by their recomplexation with $\{P_8W_{48}\}$ POT, indicating complex equilibria in aqueous solutions of **KLD-1** and **KLD-2**, which explains their very complex ^{31}P NMR spectra. This behavior is also similar to that observed previously for Sn^{II} complexes of $\{P_8W_{48}\}$, $[K_{4.5}\subset(ClSn)_8P_8W_{48}O_{184}]^{17.5-}$.[10]

Interestingly, the coordination mode of As^V centers in **3** does not allow for a significant bending-type distortion of the POT wheel, as observed in **1** and **2** (Figure 2, right). On the other hand, this results in significant distortion of the arsonate groups, as reflected by the much wider As−O bond length range in **KL-3** [$As-O_{POT}$ = 1.55(2)−1.83(3) Å; $As-O_{terminal}$ = 1.69(3) and 1.91(4) Å] compared to **KLD-1** and **KLD-2**. Another consequence is "compression" of the macrocylce toward *p*-arsanilate groups. Thus, distances between O atoms bound by As^V centers constitute 2.74−2.75 Å, while the O···O separation of the remaining four vacant sites is 3.64−3.65 Å. The "compression"-type distortion of $\{P_8W_{48}\}$ is not

DOI: 10.1021/acs.inorgchem.7b01928
Inorg. Chem. 2017, 56, 13822−13828

unprecedented and is commonly observed in its heterometal complexes, which do not possess C_4 symmetry.[7c,12]

To test the ability of using polyanions **2** as precursors for magnetic organoarsonate-functionalized $\{P_8W_{48}\}$ derivatives, we added various heterometals in solutions of **KLD-2** in an aqueous 4 M LiCl medium. The microcrystalline product **KL-4** isolated from the reactions with Fe^{III} exhibit $\{Fe_8(H_3NC_6H_4AsO)_4P_8W_{48}\}$ stoichiometry based on elemental analysis results. Unfortunately, the small crystal dimensions thus far have precluded single-crystal XRD measurements; however, the IR spectrum for **KL-4** (Figure S3) strongly supports coordination of the Fe^{III} ions to the *p*-arsanilate-functionalized polyanion (see the Supporting Information for details). This implies that **KLD-1** and **KLD-2** can act as possible novel POM precursors for organofunctionalized heterometal $\{P_8W_{48}\}$ derivatives.

4. CONCLUSIONS

In summary, we have successfully isolated the first examples of the main-group, nonmetal-element-decorated $\{P_8W_{48}\}$ derivatives with the general formula $[(RAsO)_4P_8W_{48}O_{184}]^{32-}$ [R = C_6H_5 or *p*-$(H_2N)C_6H_4$], also representing the first heteropolyoxotungstates functionalized with organoarsonates. In these species, four $\{RAs^VO\}$ moieties are connected to the POT wheel via As−O−W bonds, resulting in C_{2v}-symmetric complexes. Because of the relatively short As−O bond length compared to the M−O bonds of transition or rare-earth and Sn^{II} metal ions, the formation of $[(RAsO)_4P_8W_{48}O_{184}]^{32-}$ leads to thus-far-unprecedented distortions of the $\{P_8W_{48}\}$ wheel, which is slightly flexed toward coordinated $\{RAs^VO\}$ groups in **1** and **2**. Our solution studies revealed dissociation of the organoarsonate fragments from the title polyanions in a slightly acidic aqueous medium followed by their rearrangement within the inner POT cavity. Polyanions of the composition $[\{H_3NC_6H_4AsO\}_3P_8W_{48}O_{184}H_x\{WO_2(H_2O)_2\}_{0.4}]^{(30.2-x)-}$ (**3**) have been crystallized as the hydrated mixed K^+/Li^+ salt as the product of these structural rearrangements. At the same time, the title polyanions appear to be stable in the time frame from 1 h to at least 1 day (depending on the medium) in slightly basic solvents (pH 7.6).

The presence of vacant sites that remain noncoordinated by As^V centers in the inner cavity of the $\{P_8W_{48}\}$ macrocycle in **1**−**3** and their feasible steric accessibility open perspectives for subsequent functionalization of the organoarsonate−POM hybrids by magnetic metal centers, an avenue that we are currently investigating.

■ ASSOCIATED CONTENT

Supporting Information

The Supporting Information is available free of charge on the ACS Publications website at DOI: 10.1021/acs.inorgchem.7b01928.

Experimental details, bond length and bond-valence-sum values, and IR, Raman, and ^{31}P NMR spectra (PDF)

Accession Codes

CCDC 1548225−1548227 contain the supplementary crystallographic data for this paper. These data can be obtained free of charge via www.ccdc.cam.ac.uk/data_request/cif, or by emailing data_request@ccdc.cam.ac.uk, or by contacting The Cambridge Crystallographic Data Centre, 12 Union Road, Cambridge CB2 1EZ, UK; fax: +44 1223 336033.

■ AUTHOR INFORMATION

Corresponding Author

*E-mail: paul.koegerler@ac.rwth-aachen.de.

ORCID

Paul Kögerler: 0000-0001-7831-3953

Author Contributions

The manuscript was written through contributions of all authors. All authors have given approval to the final version of the manuscript.

Notes

The authors declare no competing financial interest.

■ ACKNOWLEDGMENTS

We gratefully acknowledge financial support by Forschungszentrum Jülich and EU ERC Starting Grant 308051-MOLSPINTRON. We thank Dr. Frank Haarmann for solid-state ^{31}P MAS NMR and Brigitte Jansen for TGA measurements.

■ REFERENCES

(1) For example, see: (a) *Chem. Soc. Rev.* **2012**, *41*, 7325−7648 (Special Issue on Polyoxometalate Cluster Science, edited by L. Cronin and Müller, A.) (b) Ji, Y. C.; Huang, L. J.; Hu, J.; Streb, C.; Song, Y. F. Polyoxometalate-functionalized nanocarbon materials for energy conversion, energy storage and sensor systems. *Energy Environ. Sci.* **2015**, *8*, 776−789. (c) Monakhov, K. Yu.; Moors, M.; Kögerler, P. Perspectives for Polyoxometalates in Single-Molecule Electronics and Spintronics, in Polyoxometalate Chemistry. *Adv. Inorg. Chem.* **2017**, *69*, 251−286. (d) Ji, Y. C.; Huang, L. J.; Hu, J.; Streb, C.; Song, Y. F. Polyoxometalate-functionalized nanocarbon materials for energy conversion, energy storage and sensor systems. *Energy Environ. Sci.* **2015**, *8*, 776−789. (e) Izarova, N. V.; Kögerler, P. Polyoxometalate-based Single-Molecule Magnets. In *Trends in Polyoxometalates Research*; Ruhlmann, L., Schaming, D., Eds.; Nova Science Publishers: Hauppauge, NY, 2015; pp 121−149.

(2) (a) Gouzerh, P.; Proust, A. Main-Group Element, Organic, and Organometallic Derivatives of Polyoxometalates. *Chem. Rev.* **1998**, *98*, 77−112. (b) Dolbecq, A.; Dumas, E.; Mayer, C. R.; Mialane, P. Hybrid Organic−Inorganic Polyoxometalate Compounds: From Structural Diversity to Applications. *Chem. Rev.* **2010**, *110*, 6009−6048. (c) Proust, A.; Matt, B.; Villanneau, R.; Guillemot, G.; Gouzerh, P.; Izzet, G. Functionalization and post-functionalization: a step towards polyoxometalate-based materials. *Chem. Soc. Rev.* **2012**, *41*, 7605−7622. (d) Song, Y. F.; Tsunashima, R. Recent advances on polyoxometalate-based molecular and composite materials. *Chem. Soc. Rev.* **2012**, *41*, 7384−7402. (e) Santoni, M.-P.; Hanan, G. S.; Hasenknopf, B. Covalent multi-component systems of polyoxometalates and metal complexes: Toward multi-functional organic−inorganic hybrids in molecular and material sciences. *Coord. Chem. Rev.* **2014**, *281*, 64−85. (f) Walsh, J. J.; Bond, A. M.; Forster, R. J.; Keyes, T. E. Hybrid polyoxometalate materials for photo(electro-)chemical applications. *Coord. Chem. Rev.* **2016**, *306*, 217−234 and references cited therein.

(3) (a) Barkigia, K. M.; Rajković, L. M.; Pope, M. T.; Quicksall, C. O. A new type of heteropolyanion. Tetramolybdo complexes of dialkyl- and diarylarsinates. *J. Am. Chem. Soc.* **1975**, *97*, 4146−4147. (b) Matsumoto, K. Y. Heteropoly anions of methylarsonate and dimethylarsinate: the crystal structures of guanidinium hexamolybdomethylarsonate hexahydrate, $(CN_3H_6)_2[CH_3AsMo_6O_{21}(H_2O)_6]\cdot 6H_2O$ and guanidinium tetramolybdodimethylarsinate monohydrate, $(CN_3H_6)_2[(CH_3)_2AsMo_4O_{14}(OH)]\cdot H_2O$. *Bull. Chem. Soc. Jpn.* **1979**, *52*, 3284−3291. (c) Barkigia, K. M.; Rajković-Blazer, L. M.; Pope, M. T.; Prince, E.; Quicksall, C. O. Molybdoarsinate heteropoly complexes. Structure of the hydrogen tetramolybdodimethylarsinate(2−) anion by X-ray and neutron diffraction. *Inorg. Chem.* **1980**, *19*, 2531−2537.

(4) (a) Kwak, W.; Rajković, L. M.; Stalick, J. K.; Pope, M. T.; Quicksall, C. O. Synthesis and structure of hexamolybdobis-

DOI: 10.1021/acs.inorgchem.7b01928
Inorg. Chem. 2017, 56, 13822−13828

(organoarsonates). *Inorg. Chem.* **1976**, *15*, 2778−2783. (b) Kwak, W.; Rajković, L. M.; Pope, M. T.; Quicksall, C. O.; Matsumoto, K. Y.; Sasaki, Y. A New molybdoarsonate. Structure of $(PhAs)_2Mo_6O_{25}H_2^{4-}$ and solution interconversion of heteropoly anions that differ by a constitutional water molecule. *J. Am. Chem. Soc.* **1977**, *99*, 6463−6464. (c) Barkigia, K. M.; Rajković-Blazer, L. M.; Pope, M. T.; Quicksall, C. O. Dodecamolybdotetrakis(organoarsonates) and the structure of a neutral zwitterionic heteropoly complex. *Inorg. Chem.* **1981**, *20*, 3318−3323. (d) Klemperer, W. G.; Schwartz, C.; Wright, D. A. Mechanistic polyoxoanion chemistry: intramolecular rearrangements of the α-$Mo_8O_{26}^{4-}$, $C_6H_5AsMo_7O_{25}^{4-}$, and $(C_6H_5As)_2Mo_6O_{24}^{4-}$ anions. *J. Am. Chem. Soc.* **1985**, *107*, 6941−6950. (e) Liu, B.; Ku, Y.; Wang, M.; Zheng, P. Synthesis and characterization of a new type of heteropolyanion: pentamolybdobis(*n*-propylarsonate), having two types of crystals under the same pH conditions in the same solution. *Inorg. Chem.* **1988**, *27*, 3868−3871. (f) Liu, B.-Y.; Xie, G.-Y.; Ku, Y.-T.; Wang, X. X-ray crystal structure of guanidinium hexamolybdobis(*o*-nitrophenylarsonate) monohydrate, $(CN_3H_6)_5[(o\text{-}NO_2C_6H_4As)_2Mo_6O_{25}H]\cdot H_2O$. *Polyhedron* **1990**, *9*, 2023−2028. (g) You, X.-Z.; Li, H.-L.; Yu, K.-B.; Li, L. Hexaaquadisodium hexakis(tetramethylammonium)bis[bis(3-acetylamino-4-hydroxyphenylarsonato) aquaoctadecaoxohexa-molybdate] decahydrate: $[Na_2(H_2O)_6][(CH_3)_4N]_6[Mo_6(C_8H_8\text{-}AsNO_5)_2O_{18}(H_2O)_2]\cdot 10H_2O$. *Acta Crystallogr.* **1993**, *C49*, 1300−1303. (h) Chang, Y.-D.; Zubieta, J. Investigations into the syntheses and structures of clusters of the Mo-O-REO_3^{2-} systems (E = P and As). *Inorg. Chim. Acta* **1996**, *245*, 177−198. (i) Johnson, B. J. S.; Buss, C. E.; Young, V. G.; Stein, A. Tetrakis(tetrabutylammonium)tetrakis-[(*p*-cyanophenyl)-trioxoarsonato]-tetratriacontaoxododecamolybdate(4−). *Acta Crystallogr., Sect. C: Cryst. Struct. Commun.* **1999**, *55*, 549−551. (j) Johnson, B. J. S.; Schroden, R. C.; Zhu, C.; Stein, A. Synthesis and characterization of 2D and 3D structures from organic derivatives of polyoxometalate clusters: role of organic moiety, counterion, and solvent. *Inorg. Chem.* **2001**, *40*, 5972−5978. (k) Johnson, B. J. S.; Schroden, R. C.; Zhu, C.; Young, V. G.; Stein, A. Design and analysis of chain and network structures from organic derivatives of polyoxometalate clusters. *Inorg. Chem.* **2002**, *41*, 2213−2218. (l) Burkholder, E.; Wright, S.; Golub, V.; O'Connor, C. J.; Zubieta, J. Solid state coordination chemistry of oxomolybdenum organoarsonate materials. *Inorg. Chem.* **2003**, *42*, 7460−7471. (m) Johnson, J B. S.; Geers, S. A.; Brennessel, W. W.; Young, V. G., Jr.; Stein, A. A coordination network containing non-coordinating polyoxometalate clusters as counterions. *Dalton Trans.* **2003**, 4678−681. (n) Tan, S.; Hobday, M.; Gorman, J.; Amiet, G.; Rix, C. Preparation and characterisation of some new Mo/O/XR (X = P or As) heteropoly blue complexes. *J. Mater. Chem.* **2003**, *13*, 1180−1185. (o) Burkholder, E.; Zubieta, J. Hydrothermal synthesis and structural characterization of a network oxide constructed from $\{Mo_{12}O_{34}(O_3AsC_6H_5)_4\}^{4-}$ clusters and $\{Cu(terpy)\}^{2+}$ subunits. *Inorg. Chim. Acta* **2004**, *357*, 301−304. (p) Dolbecq, A.; Compain, J.-D.; Mialane, P.; Marrot, J. S.; Sécheresse, F.; Keita, B.; Holzle, L. R. B.; Miserque, F.; Nadjo, L. Hexa- and dodecanuclear polyoxomolybdate cyclic compounds: application toward the facile synthesis of nanoparticles and film electrodeposition. *Chem. - Eur. J.* **2009**, *15*, 733−741. (q) Onet, C. I.; Zhang, L.; Clérac, R.; Jean-Denis, J. B.; Feeney, M.; McCabe, T.; Schmitt, W. Self-assembly of hybrid organic-inorganic polyoxomolybdates: solid-state structures and investigation of formation and core rearrangements in solution. *Inorg. Chem.* **2011**, *50*, 604−613.

(5) (a) Wasfi, S. H.; Kwak, W.; Pope, M. T.; Barkigia, K. M.; Butcher, R. J.; Quicksall, C. O. Protonation-induced dynamic stereochemistry of hexatungstobis(organoarsonate) anions. *J. Am. Chem. Soc.* **1978**, *100*, 7786−7787. (b) Jameson, G. B.; Pope, M. T.; Wasfi, S. H. The characterization of a new heteropolytungstoarsonate anion, $[CH_3AsW_7O_{27}H]^{7-}$. Topological relationships among ions related to the Lindqvist structure. *J. Am. Chem. Soc.* **1985**, *107*, 4911−4915.

(6) Contant, R.; Tézé, A. A new crown heteropolyanion, $K_{28}Li_5H_7P_8W_{48}O_{184}\cdot 92H_2O$: synthesis, structure, and properties. *Inorg. Chem.* **1985**, *24*, 4610−4614.

(7) (a) Mal, S. S.; Kortz, U. The wheel-shaped Cu_{20} tungstophosphate $[Cu_{20}Cl(OH)_{24}(H_2O)_{12}(P_8W_{48}O_{184})]^{25-}$ ion. *Angew. Chem., Int. Ed.* **2005**, *44*, 3777−3780. (b) Pichon, C.; Mialane, P.; Dolbecq, A.; Marrot, J.; Rivière, E.; Keita, B.; Nadjo, L.; Sécheresse, F. Characterization and electrochemical properties of molecular icosanuclear and bidimensional hexanuclear Cu(II) azido polyoxometalates. *Inorg. Chem.* **2007**, *46*, 5292−5301. (c) Sousa, F. L.; Bögge, H.; Merca, A.; Gouzerh, P.; Thouvenot, R.; Müller, A. Vectorial growth/regulations in a $\{P_8W_{48}\}$-type polyoxotungstate compartment: trapped unusual molybdenum oxide acts as a handle. *Chem. Commun.* **2009**, 7491−7493.

(8) Mitchell, S. G.; Streb, C.; Miras, H. N.; Boyd, T.; Long, D.-L.; Cronin, L. Face-directed self-assembly of an electronically active Archimedean polyoxometalate architecture. *Nat. Chem.* **2010**, *2*, 308−312.

(9) Zhan, C.; Cameron, J. M.; Gabb, D.; Boyd, T.; Winter, R. S.; Vilà-Nadal, L.; Mitchell, S. G.; Glatzel, S.; Breternitz, J.; Gregory, D. H.; Long, D.-L.; Macdonell, A.; Cronin, L. A metamorphic inorganic framework that can be switched between eight single-crystalline states. *Nat. Commun.* **2017**, *8*, 14185.

(10) Izarova, N. V.; Klass, L.; de Oliveira, P.; Mbomekalle, I. M.; Peters, V.; Haarmann, F.; Kögerler, P. Tin(II)-functionalization of the archetypal $\{P_8W_{48}\}$ polyoxotungstate. *Dalton Trans.* **2015**, *44*, 19200−19206.

(11) (a) Brown, I. D.; Altermatt, D. Bond-valence parameters obtained from a systematic analysis of the Inorganic Crystal Structure Database. *Acta Crystallogr., Sect. B: Struct. Sci.* **1985**, *41*, 244−247. (b) Knížek, K. *Kalvados—Software for crystal structure and powder diffraction*; http://www.fzu.cz/~knizek/kalvados/index.htmlhttp://www.fzu.cz/~knizek/kalvados/index.html.

(12) For example, see: (a) Mal, S. S.; Nsouli, N. H.; Dickman, M. H.; Kortz, U. Organoruthenium derivative of the cyclic $[H_7P_8W_{48}O_{184}]^{33-}$ anion: $[\{K(H_2O)\}_3\{Ru(p\text{-cymene})(H_2O)\}_4P_8W_{49}O_{186}(H_2O)_2]^{27-}$. *Dalton Trans.* **2007**, 2627−2630. (b) Müller, A.; Pope, M. T.; Todea, A. M.; Bögge, H.; van Slageren, J.; Dressel, M.; Gouzerh, P.; Thouvenot, R.; Tsukerblat, B.; Bell, A. Metal-Oxide-Based Nucleation Process under Confined Conditions: Two Mixed-Valence V_6-Type Aggregates Closing the W_{48} Wheel-Type Cluster Cavities. *Angew. Chem., Int. Ed.* **2007**, *46*, 4477−4480. (c) Bassil, B. S.; Ibrahim, M.; Mal, S. S.; Suchopar, A.; Biboum, R. N.; Keita, B.; Nadjo, L.; Nellutla, S.; van Tol, J.; Dalal, N. S.; Kortz, U. Cobalt, Manganese, Nickel, and Vanadium Derivatives of the Cyclic 48-Tungsto-8-Phosphate $[H_7P_8W_{48}O_{184}]^{33-}$. *Inorg. Chem.* **2010**, *49*, 4949−4959.

DOI: 10.1021/acs.inorgchem.7b01928
Inorg. Chem. 2017, 56, 13822−13828